Supporting Information for:

Controlled synthesis and exploration of Cu_xFeS_4 bornite nanocrystals

*Joshua C. Kays[†], Carl R. Conti III[‡], Artemis Margaronis[†], Jason E. Kuszynski[‡], Geoffrey F. Strouse[‡], and Allison M. Dennis[†§]**

[†] Department of Biomedical Engineering, Boston University, Boston MA 02215.
[‡] Department of Chemistry and Biochemistry, Florida State University, Tallahassee FL 32306.
[§] Division of Materials Science & Engineering, Boston University, Boston MA 02215.

Email: aldennis@bu.edu

Contents

Note 1: LSPR modeling

The LSPR of each sample was fit using a simple Drude model with previously described MATLAB code.[1] The literature value for the high frequency dielectric constant of bornite was used for Drude fitting.[2] A frequency independent damping constant was utilized for fittings, leading to the following equations:

$$\chi(\omega) = \varepsilon_\infty + \chi_{BG}(\omega) + \chi_{UV}(\omega) + \chi_D(\omega) \quad (1)$$

$$\chi_D(\omega) = -\frac{\omega_p^2}{\omega^2 + i\omega\Gamma} \quad (2)$$

where ε_∞ is the high frequency dielectric constant of the sample, χ_{BG} is the background susceptibility, which is a sum of the solvent and ligand indices of refraction, χ_{UV} represents the absorption in the conduction band, which is negligible in the frequency range fitted here, χ_D is the Drude susceptibility, ω is the frequency, ω_p is the plasma frequency, and Γ is the frequency independent damping constant. Values of 3.48, 1.51, and 1.46 were used for the high frequency dielectric constant of the nanocrystal, the refractive index of the solvent, and the refractive of the ligand, respectively.[1,2]

The effective mass for each sample was then calculated using the plasma frequency (as determined by fitting the LSPR using the Drude model), the chemical titration determined carrier density, and the following equation:

$$\omega_p = \sqrt{\frac{ne^2}{m^*\varepsilon_0}} \quad (3)$$

where n is the free carrier concentration, e is the charge of the free carrier, m^* is the effective mass of the free carrier, and ε_0 is the vacuum permittivity constant.

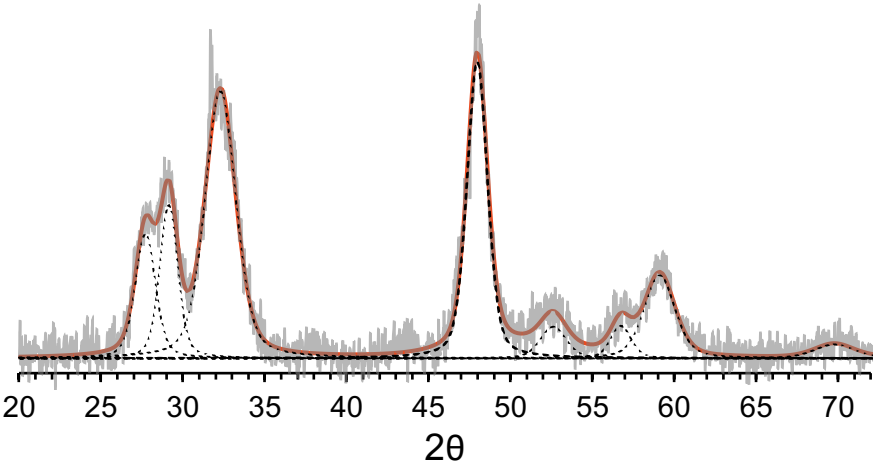

Figure S1: XRD of DDT free reaction. Peaks at 52.5°, 59°, and doublet around 28° are distinctive covellite peaks.

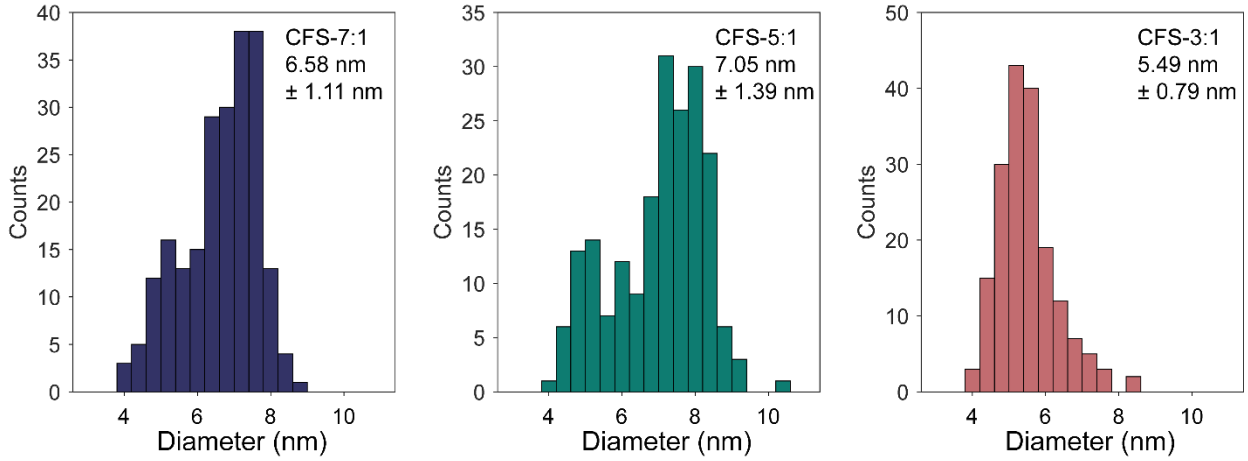

Figure S2: TEM histogram of CFS-7:1, 5:1, and 3:1.

Table S1: Impact of iron content on d-spacing.

Iron content (% of cations)	8.8%	11.8%	16.4%	25.0%	28.1%
<1 1 1> plane (~28° 2θ)	3.178	3.180	3.163	3.160	3.151
<2 0 0> plane (~32° 2θ)	2.758	2.754	2.741	2.742	2.718
<2 2 0> plane (~47° 2θ)	1.944	1.941	1.930	1.911	1.911
<3 1 1> plane (~56° 2θ)	1.658	1.655	1.650	1.623	1.610

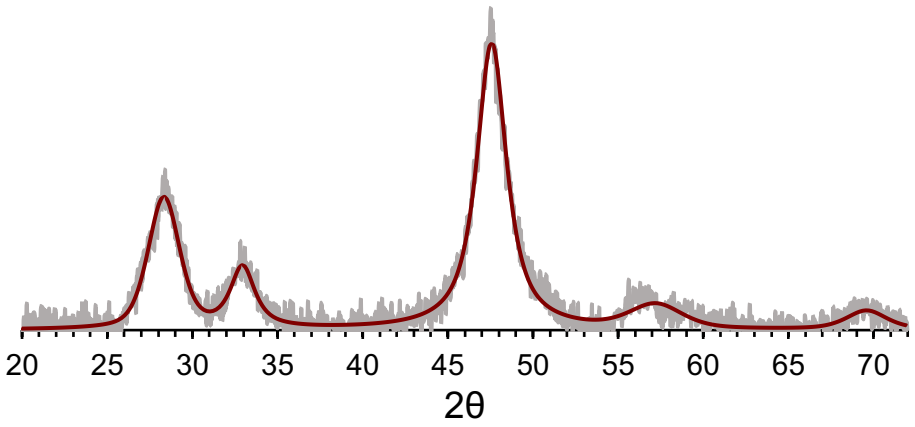

Figure S3: XRD of 2.6:1 Cu:Fe bornite. Peaks of high iron content sample match the bornite reference (AMCSD 0000048) peaks at 28.3°, 32.7°, 46.9°, and 68.6° 2θ (see Figure 1C for reference). Importantly, the absence of chalcopyrite reference peaks (29.4° highest intensity, 49° second highest, AMCSD 0009476) suggest phase purity.

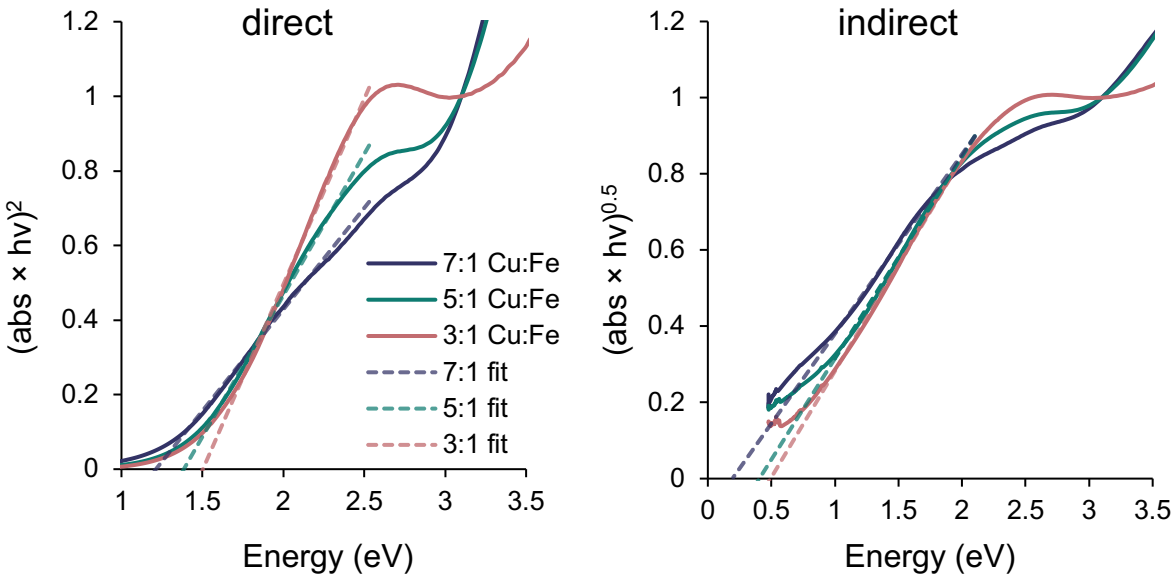

Figure S4: Tauc plots of 7:1, 5:1 and 3:1 bornite. Dashed lines indicate the linear fits used to extrapolate to axis and estimate the band gap.

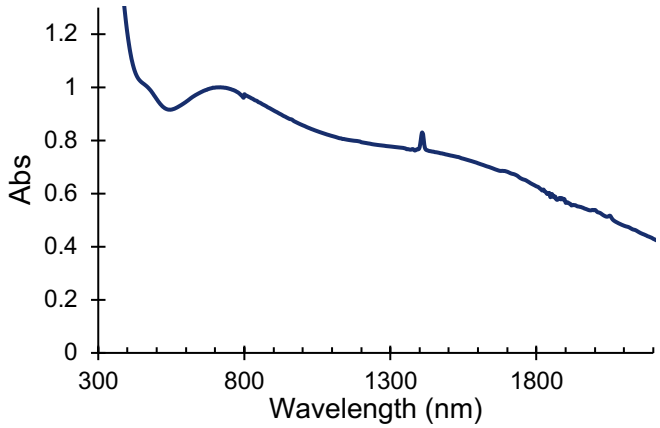

Figure S5: Absorbance of air-free 10:1 Cu:Fe bornite NCs. Low iron content bornite still shows similar absorbance to other bornite and does not show infrared LSPR until it is exposed to oxygen, in contrast to recent literature.[3]

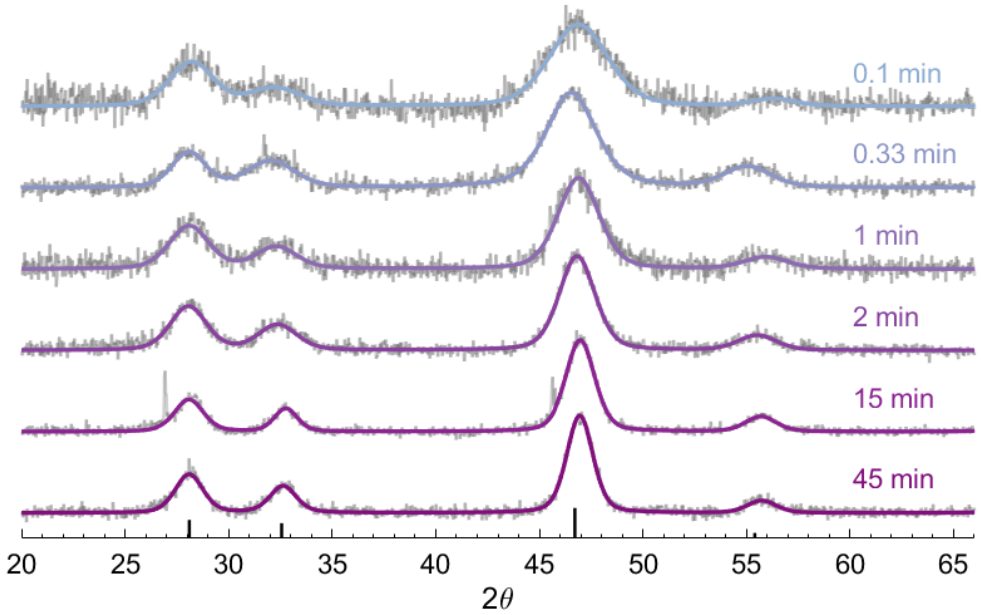

Figure S6: XRD of bornite growth over time.

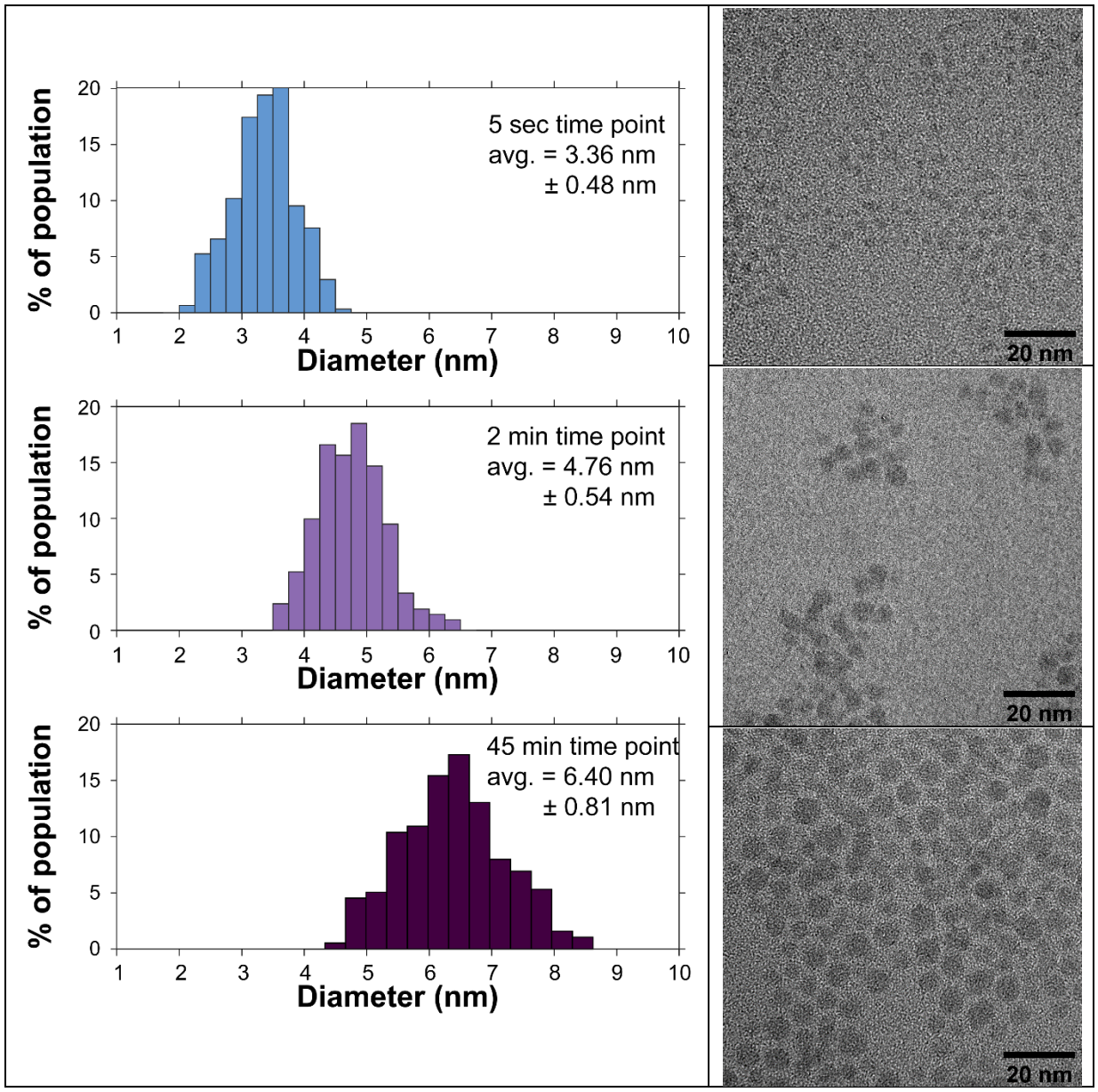

Figure S7: TEM of size series. For all samples, 200 or more NCs were sized for the histograms.

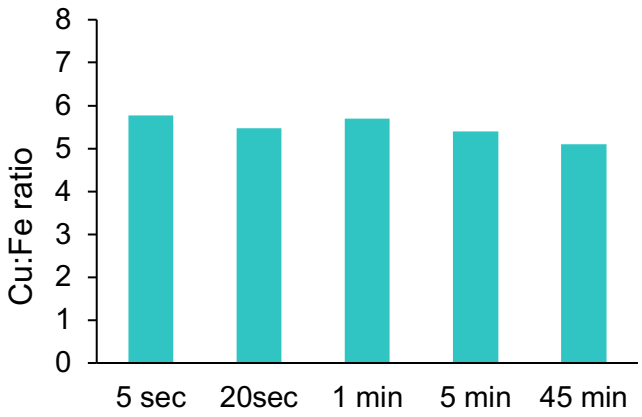

Figure S8: Cu:Fe ratio of bornite size series grown over time. Measured Cu:Fe content of a selection from the bornite size series in Figure 1F, determined by MP-AES.

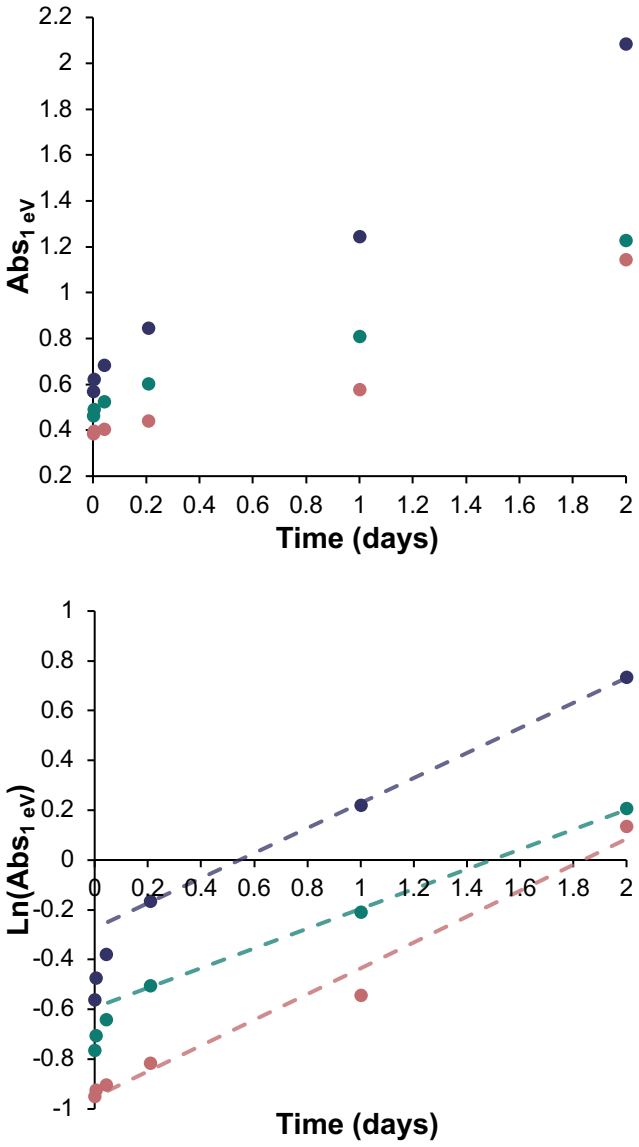

Figure S9: Kinetics of oxidation. Top is raw absorbance at 1 eV over time, bottom is the natural logarithm of that data over time. Lines in bottom fit indicate the linear region, implying 1st order kinetics.

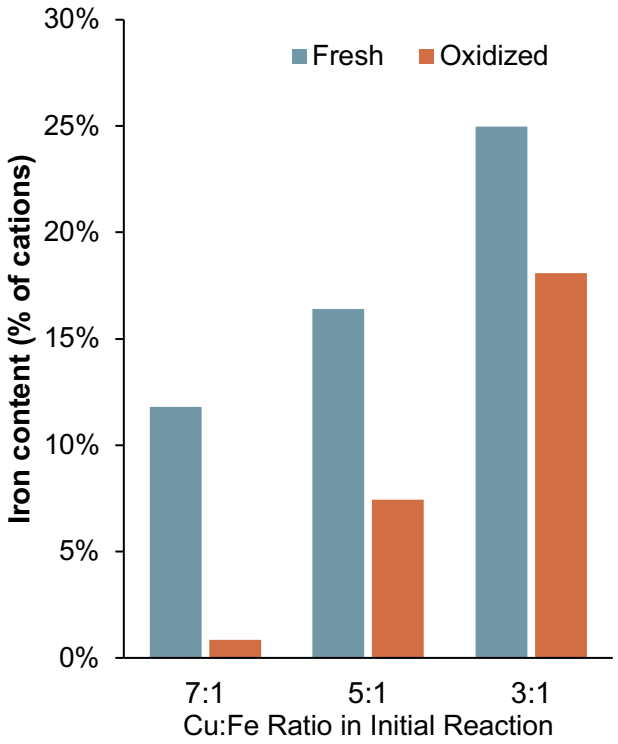

Figure S10: Impact of oxidation on iron content. MP-AES analysis of samples before and after oxidation.

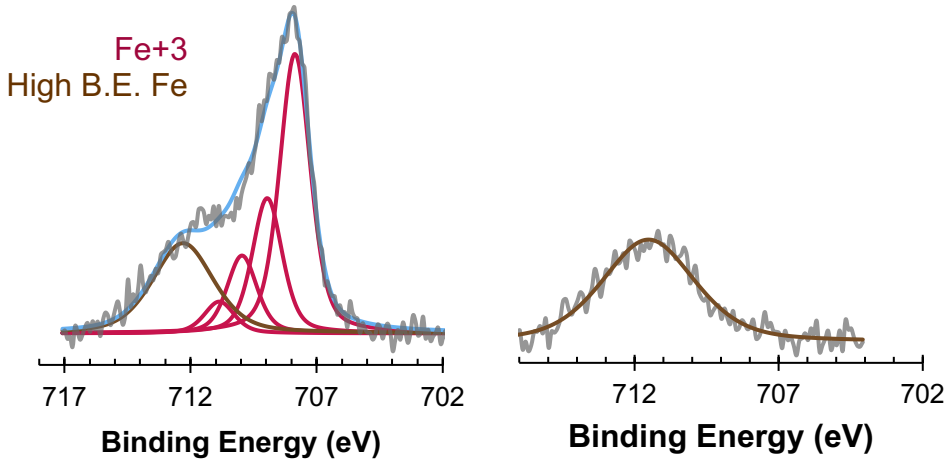

Figure S11: XPS of iron 2p 3/2 peaks, Shirley background subtracted. For clarity, this is the same data as Figure 4 C,D, but with the Shirley background subtracted. Left is fresh bornite, right is oxidized. The Fe^{+3} peak is fit to a multiplet with fixed positions and areas per literature.[4]

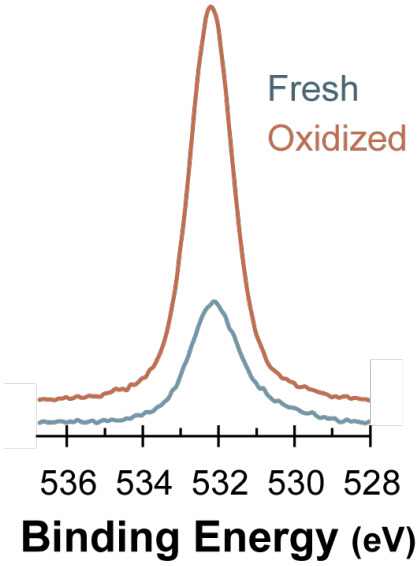

Figure S12: XPS of oxygen (1s spectrum). Axis offset for clarity.

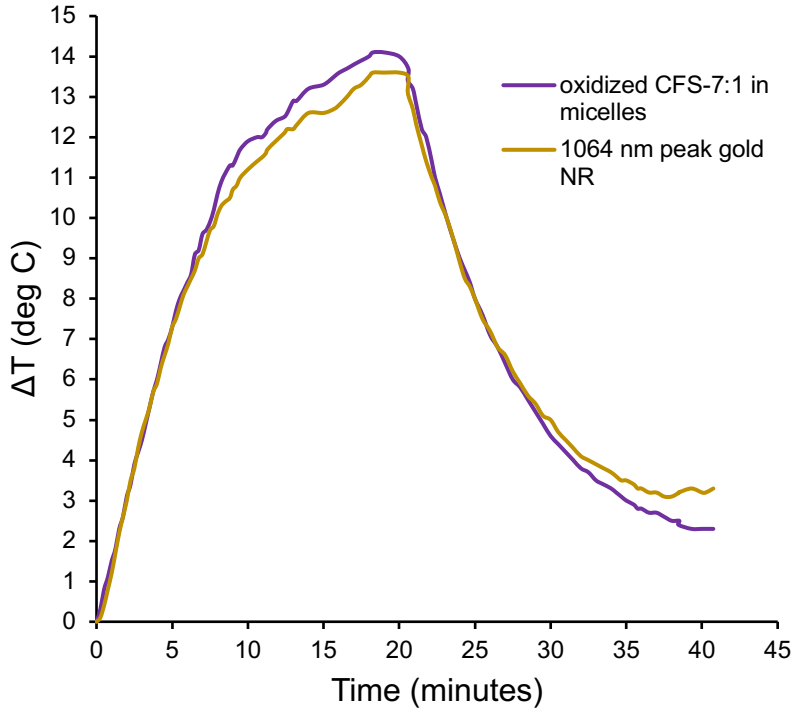

Figure S13: Oxidized CFS performs similarly to gold nanorods as a photothermal mediator. 1 mL of 27 µg/mL oxidized CFS-7:1 or gold NRs in a quartz cuvette was illuminated with a 0.7 W output power 1050nm LED from Ushio. After 20 min, the LED was turned off and samples cooled naturally. Data offset by subtracting t=0 temperature (~20°C) for both samples.

References

(1) Mendelsberg, R. J.; Garcia, G.; Milliron, D. J. Extracting Reliable Electronic Properties from Transmission Spectra of Indium Tin Oxide Thin Films and Nanocrystal Films by Careful Application of the Drude Theory. *J. Appl. Phys.* **2012**, *111* (6), 063515. https://doi.org/10.1063/1.3695996.

(2) Sil, S.; Datta, J.; Das, M.; Jana, R.; Halder, S.; Biswas, A.; Sanyal, D.; Ray, P. P. Bias Dependent Conduction and Relaxation Mechanism Study of Cu5FeS4 Film and Its Significance in Signal Transport Network. *J. Mater. Sci. Mater. Electron.* **2018**, *29* (6), 5014–5024. https://doi.org/10.1007/s10854-017-8463-4.

(3) Lee, S.; Ghosh, S.; Hoyer, C. E.; Liu, H.; Li, X.; Holmberg, V. C. Iron-Content-Dependent, Quasi-Static Dielectric Resonances and Oxidative Transitions in Bornite and Chalcopyrite Copper Iron Sulfide Nanocrystals. *Chem. Mater.* **2021**, *33* (5), 1821–1831. https://doi.org/10.1021/acs.chemmater.0c04798.

(4) Grosvenor, A. P.; Kobe, B. A.; Biesinger, M. C.; McIntyre, N. S. Investigation of Multiplet Splitting of Fe 2p XPS Spectra and Bonding in Iron Compounds. *Surf. Interface Anal.* **2004**, *36* (12), 1564–1574. https://doi.org/10.1002/sia.1984.